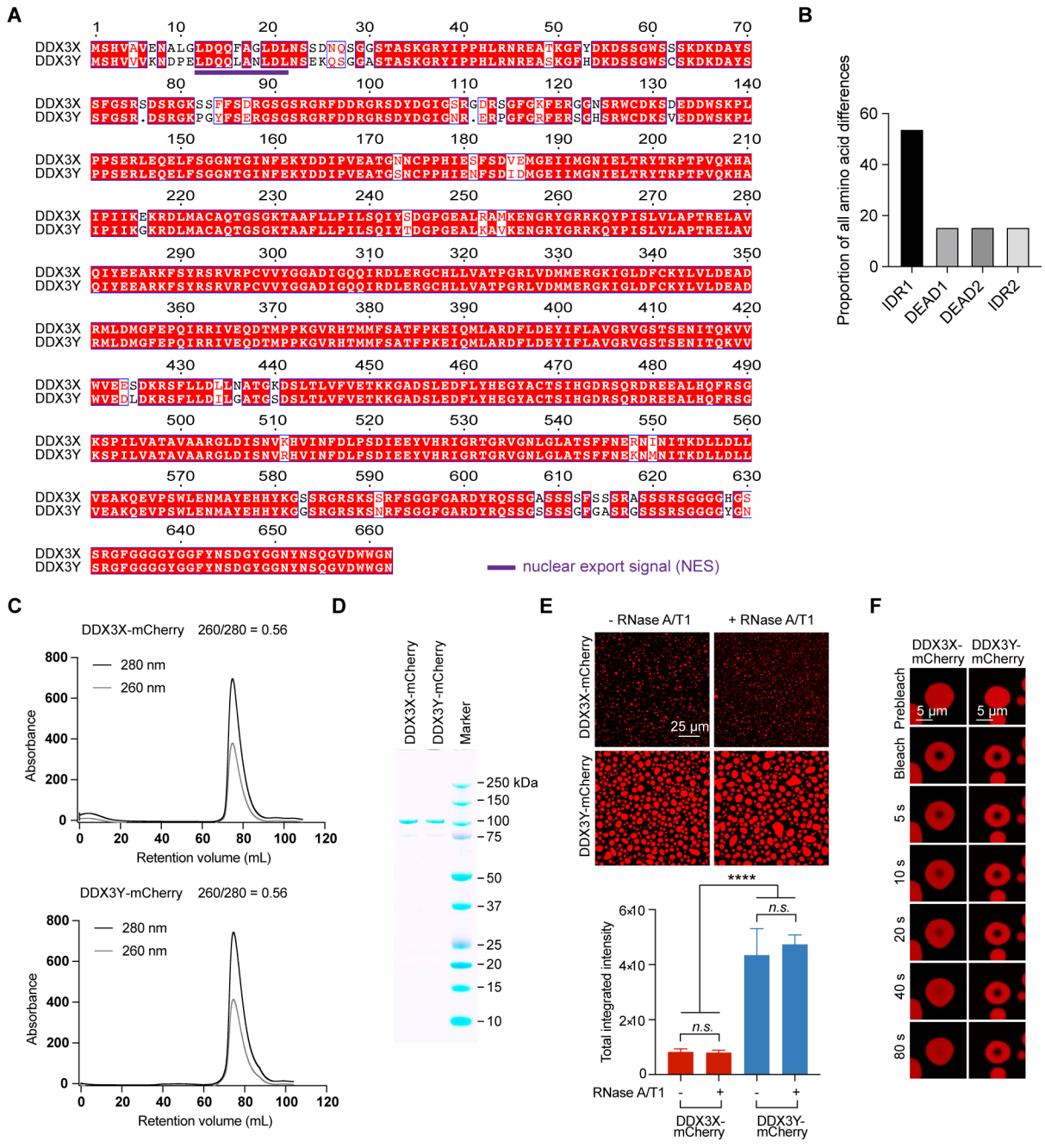
A
DDX3X
DDX3Y
nuclear export signal (NES)
B
Proportion of all amino acid differences
IDR1
DEAD1
DEAD2
IDR2
C
DDX3X-mCherry 260/280 = 0.56
DDX3Y-mCherry 260/280 = 0.56
280 nm
260 nm
Absorbance
Retention volume (mL)
D
DDX3X-mCherry
DDX3Y-mCherry
Marker
250 kDa
150
100
75
50
37
25
20
15
10
E
- RNase A/T1
+ RNase A/T1
25 μm
Total integrated intensity
****
n.s.
RNase A/T1
F
Prebleach
Bleach
5 s
10 s
20 s
40 s
80 s
5 μm

Figure S1 DDX3Y has a stronger LLPS propensity compared to DDX3X *in vitro*. Related to Figure 1. (A) Amino acid sequence alignment of human DDX3X and DDX3Y. The nuclear export signal (NES) is underlined in purple. (B) Percentage of sequence differences attributable to the individual domains (IDR1, DEAD1, DEAD2, and IDR2) between DDX3X and DDX3Y. (C) Chromatographic profiles of the purification of DDX3X-mCherry and DDX3Y-mCherry. The black line refers to A_{280nm}, and the gray line refers to A_{260nm}. The final A_{260nm}/A_{280nm} was determined using a Nanodrop spectrophotometer. The ratios of A_{260nm}/A_{280nm} of DDX3X and DDX3Y indicate that the purified proteins don't contain noticeable RNA carry-over. (D) SDS-PAGE results of purified DDX3X-mCherry and DDX3Y-mCherry proteins. (E) Top: *in vitro* droplet formation of 10 μM recombinant DDX3X-mCherry or DDX3Y-mCherry, with or without RNase treatment, in the presence of 200 ng/μL poly(U)-RNA. Scale bar, 25 μm. Bottom: quantification of the total integrated intensity of DDX3X condensation and DDX3Y condensation from the top panel. A two-tailed t-test was used to calculate the *p*-values between +/- RNase treatment. A nested t-test was used to calculate the *p*-value between DDX3X and DDX3Y groups; *n.s.* $p > 0.05$, ****$p < 0.0001$. (F) One representative biological replicate of Figure 1F. Size-comparable droplets of DDX3X and DDX3Y were chosen. Time-lapse images of the DDX3X-mCherry (10 μM) and DDX3Y-mCherry (10 μM) droplets from *in vitro* FRAP experiments.

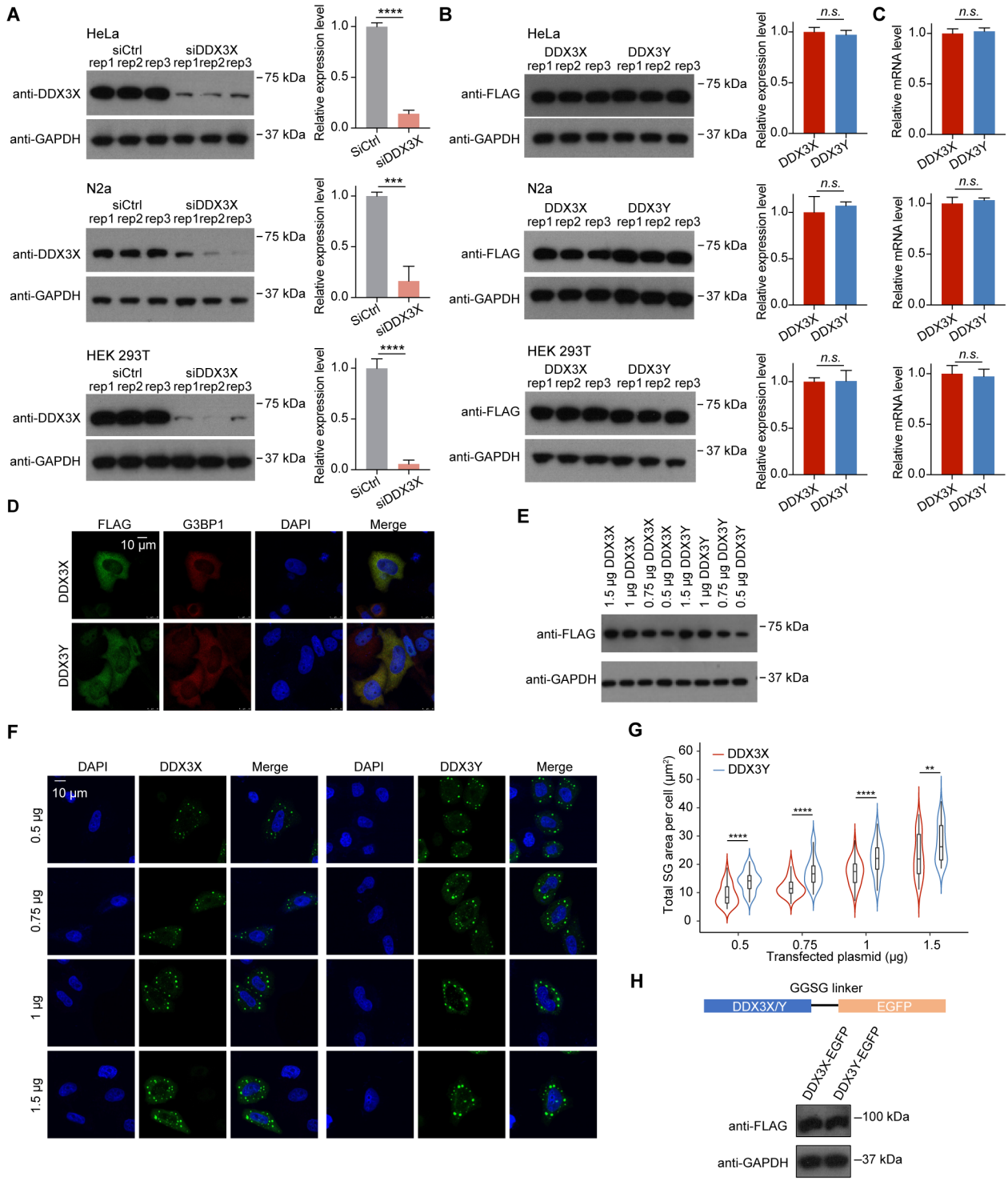
A
HeLa
siCtrl rep1 rep2 rep3
siDDX3X rep1 rep2 rep3
anti-DDX3X
anti-GAPDH
75 kDa
37 kDa
Relative expression level
SiCtrl
siDDX3X
N2a
HEK 293T
B
DDX3X rep1 rep2 rep3
DDX3Y rep1 rep2 rep3
anti-FLAG
n.s.
C
Relative mRNA level
DDX3X
DDX3Y
D
FLAG
G3BP1
DAPI
Merge
10 μm
E
1.5 μg DDX3X
1 μg DDX3X
0.75 μg DDX3X
0.5 μg DDX3X
1.5 μg DDX3Y
1 μg DDX3Y
0.75 μg DDX3Y
0.5 μg DDX3Y
F
0.5 μg
0.75 μg
1 μg
1.5 μg
G
Total SG area per cell (μm²)
Transfected plasmid (μg)
H
GGSG linker
DDX3X/Y
EGFP
DDX3X-EGFP
DDX3Y-EGFP
100 kDa

Figure S2 DDX3Y has a stronger LLPS propensity compared to DDX3X in cells. Related to Figure 2. (A) Western blots showing the expression of DDX3X in DDX3X-knockdown and knockdown control HeLa, N2a, and HEK 293T cells. The intensity of each band was quantified using Fiji. The intensity of each DDX3X band was normalized to the corresponding GAPDH intensity and then normalized to the knockdown control samples. Error bars represent s.d. of three biological replicates. *p* values were determined by a two-tailed t-test; *** $p < 0.001$; **** $p < 0.0001$. (B) Western blot results show that FLAG-DDX3X and FLAG-DDX3Y are expressed at comparable levels in HeLa, N2a, and HEK 293T cells. The intensity of each band was quantified using Fiji. The intensity of each DDX3X or DDX3Y band was normalized to the corresponding GAPDH intensity and then normalized to the DDX3X overexpression samples. Error bars represent s.d. of three biological replicates. *p* values were determined by a two-tailed t-test; *n.s.* $p > 0.05$. (C) RT-qPCR results show that the transcript level of DDX3X and DDX3Y were comparable in HeLa, N2a, and HEK 293T cells. Each sample was normalized to the corresponding loading control GAPDH first and then normalized to DDX3X. *p* values were determined by a two-tailed t-test; *n.s.* $p > 0.05$. (D) Representative images of FLAG-DDX3X or FLAG-DDX3Y localization with G3BP1 in HeLa cells before arsenite treatment. The expression of FLAG-DDX3X and FLAG-DDX3Y did not lead to puncta formation for this condition. Scale bar, 10 μm. (E) Western blot results showing the expression level of DDX3X and DDX3Y in HeLa cells transfected with different amounts of plasmids. (F) Immunofluorescent cell stain of SGs formed by different amounts of DDX3X and DDX3Y. The SGs were triggered by 500 μM sodium arsenite for 1 hr. Scale bar, 10 μm. (G) The total SG area per cell were quantified (n = 50 cells in total, from three biologically independent experiments) and displayed in violin plots. *p* values were determined by a two-tailed t-test; ** $p < 0.01$, **** $p < 0.0001$. (H) Construct and expression of DDX3X-EGFP and DDX3Y-EGFP in HeLa cells. A GlyGlySerGly (GGSG) linker was inserted between DDX3X/Y and EGFP.

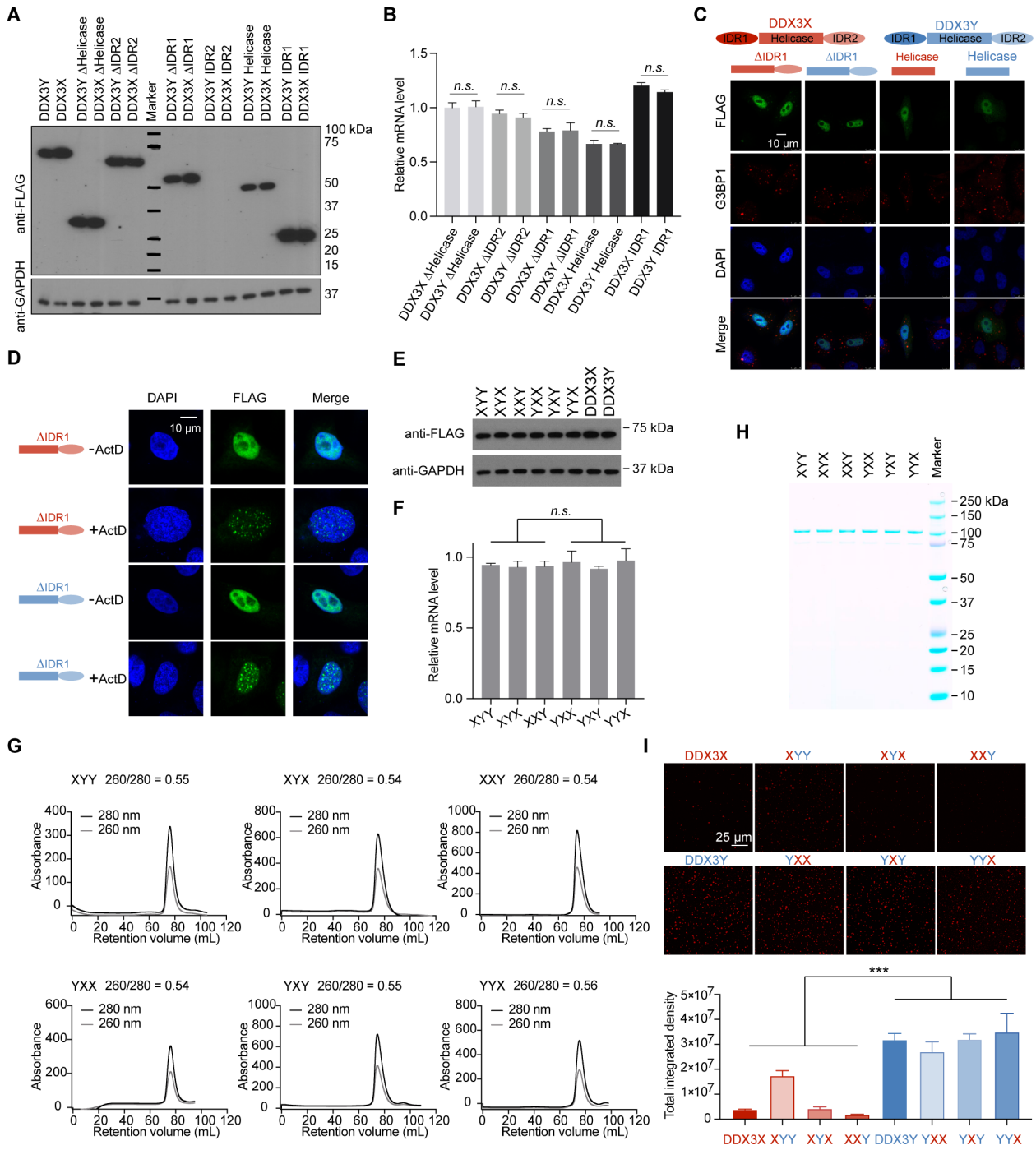
A
DDX3Y
DDX3X
DDX3Y ΔHelicase
DDX3X ΔHelicase
DDX3Y ΔIDR2
DDX3X ΔIDR2
Marker
DDX3Y ΔIDR1
DDX3X ΔIDR1
DDX3Y IDR2
DDX3X IDR2
DDX3Y Helicase
DDX3X Helicase
DDX3Y IDR1
DDX3X IDR1
100 kDa
75
50
37
25
20
15
anti-FLAG
anti-GAPDH
37
B
Relative mRNA level
1.5
1.0
0.5
0.0
n.s.
DDX3X ΔHelicase
DDX3Y ΔHelicase
DDX3X ΔIDR2
DDX3Y ΔIDR2
DDX3X ΔIDR1
DDX3Y ΔIDR1
DDX3X Helicase
DDX3Y Helicase
DDX3X IDR1
DDX3Y IDR1
C
DDX3X
IDR1
Helicase
IDR2
ΔIDR1
ΔIDR1
DDX3Y
IDR1
Helicase
IDR2
Helicase
Helicase
FLAG
G3BP1
DAPI
Merge
10 μm
D
DAPI
FLAG
Merge
ΔIDR1
-ActD
ΔIDR1
+ActD
ΔIDR1
-ActD
ΔIDR1
+ActD
10 μm
E
XYY
XYX
XXY
YXX
YXY
YYX
DDX3X
DDX3Y
anti-FLAG
anti-GAPDH
75 kDa
37 kDa
F
n.s.
Relative mRNA level
1.0
0.5
0.0
XYY
XYX
XXY
YXX
YXY
YYX
H
XYY
XYX
XXY
YXX
YXY
YYX
Marker
250 kDa
150
100
75
50
37
25
20
15
10
G
XYY 260/280 = 0.55
XYX 260/280 = 0.54
XXY 260/280 = 0.54
YXX 260/280 = 0.54
YXY 260/280 = 0.55
YYX 260/280 = 0.56
280 nm
260 nm
Absorbance
Retention volume (mL)
I
DDX3X
XYY
XYX
XXY
DDX3Y
YXX
YXY
YYX
25 μm
***
Total integrated density
5×10^7
4×10^7
3×10^7
2×10^7
1×10^7
0
DDX3X XYY
XYX
XXY
DDX3Y YXX
YXY
YYX

Figure S3 IDR1 of DDX3Y more strongly promotes phase separation than IDR1 of DDX3X. Related to Figure 3. (A) Western blot results showing the expression of the wild type and truncated variants of DDX3X (including DDX3X$^{\Delta helicase}$, DDX3X$^{\Delta IDR2}$, DDX3X$^{\Delta IDR1}$, DDX3X^{IDR2}, DDX3X^{helicase}, DDX3X^{IDR1}) and DDX3Y (including DDX3Y$^{\Delta helicase}$, DDX3Y$^{\Delta IDR2}$, DDX3Y$^{\Delta IDR1}$, DDX3Y^{IDR2}, DDX3Y^{helicase}, DDX3Y^{IDR1}). The IDR2 domains alone do not express in HeLa cells. (B) RT-qPCR to show the transcript level of different DDX3X and DDX3Y truncations. All the truncations were normalized to the loading control GAPDH first and then normalized to DDX3X. DDX3X truncations were expressed at the comparable level to the corresponding DDX3Y truncations. *p* values were determined by a two-tailed t-test; *n.s.* $p > 0.05$. (C) Representative images of localization of DDX3$^{\Delta IDR1}$, DDX3Y$^{\Delta IDR1}$, DDX3X^{helicase}, DDX3Y^{helicase}, and G3BP1 in HeLa cells upon arsenite treatment (500 μm, 1 hr). Scale bar, 10 μm. (D) Representative images of localization of DDX3$^{\Delta IDR1}$ and DDX3Y$^{\Delta IDR1}$ with and without 5 μg/mL of actinomycin D (ActD) treatment for 2 hrs. Scale bar, 10 μm. (E) Western blot results showing the expression of the wild type and domain-swap variants of DDX3X and DDX3Y. (F) RT-qPCR to show the transcript level of different DDX3X and DDX3Y domain-swap variants. All the truncations were normalized to the loading control GAPDH first and then normalized to DDX3X. All the domain-swap variants were expressed at the comparable level. *p* values were determined by a two-tailed t-test; *n.s.* $p > 0.05$. (G) Chromatographic profile of the domain-swap variants with mCherry tag during purification. The black line refers to A_{280nm}, and the gray line refers to A_{260nm}. The final A_{260nm}/A_{280nm} was determined using a Nanodrop spectrophotometer. The ratios of A_{260nm}/A_{280nm} of DDX3X and DDX3Y indicate that the purified proteins don't contain noticeable RNA carryover. (H) SDS-PAGE gel of the final purified the domain-swap variants with mCherry tag. (I) *In vitro* droplet formation of 7.5 μM recombinant DDX3X-mCherry, DDX3Y-mCherry, and domain swap variants of DDX3X and DDX3Y in the absence of poly(U)-RNA. Scale bar, 25 μm. Quantification of the total integrated intensity of the different types of condensations. Error bars represent s.d. from three repeats at

each condition. *p* values were determined by nested t-test in the Prism to compare all domain-swapped variants with X^{IDR1} versus all domain-swapped variants with Y^{IDR1}; ***$p < 0.001$.

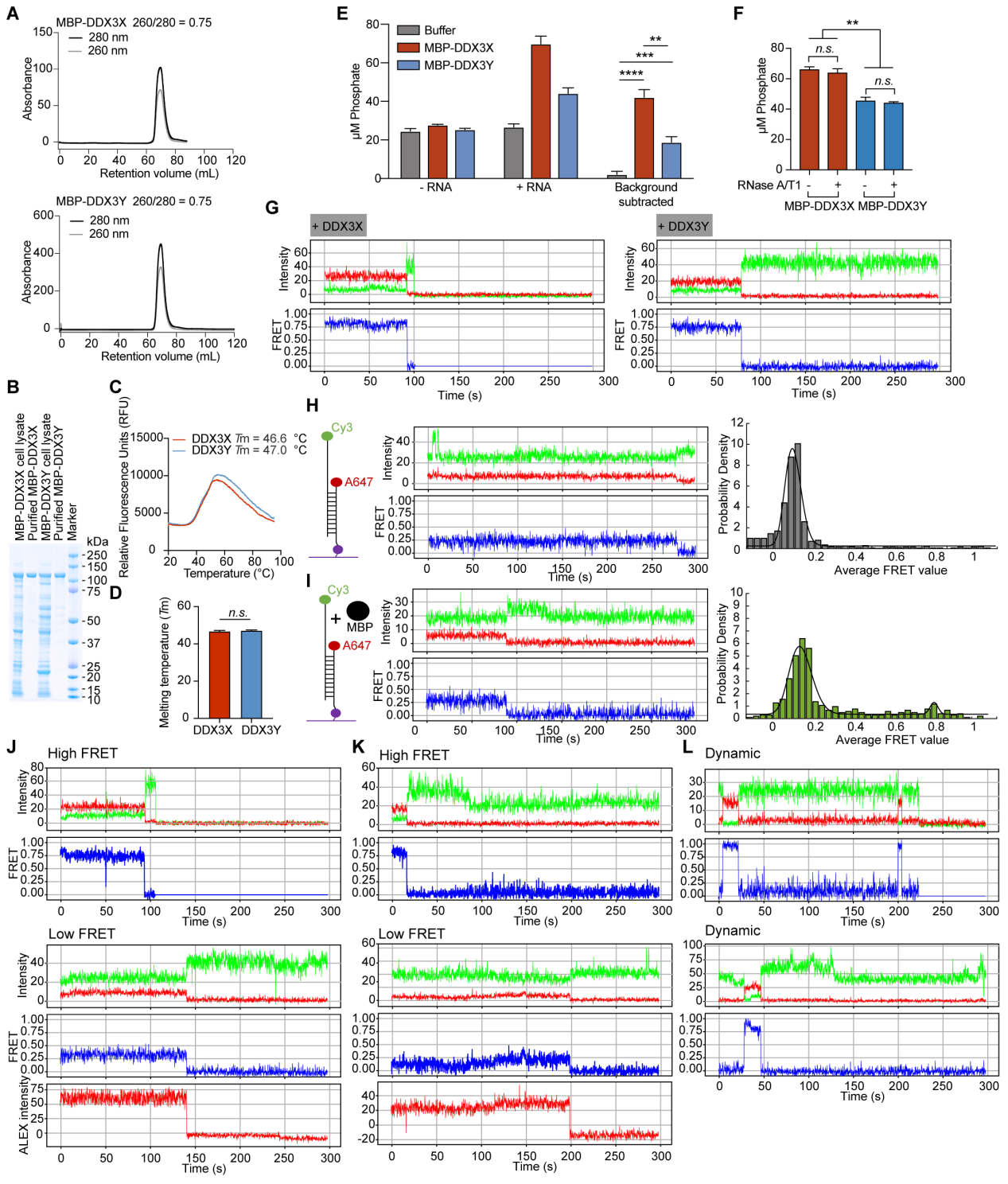
A
MBP-DDX3X 260/280 = 0.75
280 nm
260 nm
Absorbance
Retention volume (mL)
MBP-DDX3Y 260/280 = 0.75
B
MBP-DDX3X cell lysate
Purified MBP-DDX3X
MBP-DDX3Y cell lysate
Purified MBP-DDX3Y
Marker
kDa
C
Relative Fluorescence Units (RFU)
DDX3X Tm = 46.6 °C
DDX3Y Tm = 47.0 °C
Temperature (°C)
D
Melting temperature (Tm)
n.s.
DDX3X
DDX3Y
E
Buffer
MBP-DDX3X
MBP-DDX3Y
μM Phosphate
- RNA
+ RNA
Background subtracted
F
n.s.
RNase A/T1
MBP-DDX3X MBP-DDX3Y
G
+ DDX3X
+ DDX3Y
Intensity
FRET
Time (s)
H
Cy3
A647
Probability Density
Average FRET value
I
MBP
J
High FRET
Low FRET
ALEX intensity
K
L
Dynamic

Figure S4 The weaker ATPase activity of DDX3Y compared to DDX3X weakens its condensate disassembly. Related to Figure 4. (A) Chromatographic profile of MBP-DDX3X and MBP-DXDX3Y during purification. The black line refers to A_{280nm}, and the gray line refers to A_{260nm}. The final A_{260nm}/A_{280nm} ratio was determined using a Nanodrop spectrophotometer. (B) SDS-PAGE gel of the bacterial cell lysate and the final purified MBP-DDX3X and MBP-DDX3Y. (C) Differential Scanning Fluorometry (DSF) melting curves showing the relative fluorescence units with increasing temperature. The fluorescence is a product of SYPRO Orange dye, which resides on hydrophobic residues of exposed residues of DDX3X/DDX3Y and has a max fluorescence at 620 nm. The steady increase in fluorescence is due to the unfolding of the protein with increased temperature and the subsequent binding of the SYPRO Orange dye. (D) The melting temperatures (*Tm*, the temperature at which 50% of a protein sample is in a folded and 50% is in an unfolded state) of MBP-DDX3X and MBP-DDX3Y determined by DSF. *p* values were determined by a two-tailed t-test; *n.s.* $p > 0.05$. (E) Malachite green ATPase assay. Reactions were assembled as described in methods. Measurements were taken with 1.0 μM MBP-DDX3X, MBP-DDX3Y, or buffer with 2 mM ATP either in the absence of RNA ("- RNA") or with the addition of 100 ng/μL total HeLa RNA ("+ RNA") to stimulate ATPase activity after a 30 min reaction. "- RNA" values were subtracted from their corresponding "+ RNA" values as background ("Background Subtracted"). Values = mean ± s.d., n = 3 repeats. (F) Malachite green ATPase assays of MBP-DDX3X and MBP-DDX3Y with or without RNase treatment. Values = mean ± s.d., n = 3 repeats. A two-tailed t-test was used to calculate the *p*-values between +/- RNase treatment; a nested t-test was used to calculate the *p*-value between DDX3X and DDX3Y groups; *n.s.* $p > 0.05$, $^{**}p < 0.01$. (G) – (L) Recordings of single-molecule fluorescence intensities excited at 532 nm, corrected for channel sensitivities and spectral bleed-through as described in Methods. Green, Cy3 donor fluorescence; red, sensitized emission of Alexa 647 due to FRET; blue FRET Efficiency. The sudden decrease of the Alexa 647 and FRET traces accompanied by an increase of Cy3 intensity in each panel indicates photobleaching of the Alexa 647. Photobleaching of Alexa

647 was corroborated by direct excitation in alternating frames at 640 nm. (G) Representative fluorescent intensities and the FRET efficiency of RNA probe with MBP-DDX3X (left) and MBP-DDX3Y (right), which show high FRET. The histograms of FRET efficiencies are shown in Figure 4E. (H) The RNA probe alone gave low FRET, with a peak at E = ~0.12. Left panel: schematic of the RNA construct immobilized on the coverslip surface. Middle panel: representative figure showing the raw traces of the fluorescent intensities and the FRET efficiency trace. Right panel: histogram showing the distribution of FRET efficiencies from ~1000 traces. (I) The RNA probe with MBP (a control with no DDX3), gave low FRET, like the RNA probe alone. Left panel: schematic of the FRET assay configuration. Middle panel: representative plot showing the raw traces of the fluorescent intensities and the FRET efficiency trace. Right panel: histogram figure showing the distribution of FRET efficiency from ~400 traces, similar to the RNA in the absence of MBP. (J) Corresponding fluorescent intensities and FRET efficiency of the RNA probe with MBP-DDX3X and 1 mM ATP show high FRET and low FRET. The histogram is shown in Figure 4E. The lower panel of the low FRET trace shows ALEX direct excitation of Alexa 647 at 640 nm, indicating both donor and acceptor are present. (K) Corresponding fluorescent intensities and FRET efficiency of the RNA probe with MBP-DDX3Y and 1 mM ATP show high FRET and low FRET. The histogram is shown in Figure 4E. The lower panel of the low FRET trace shows ALEX direct excitation of Alexa 647, indicating both donor and acceptor are present. (L) Examples of corresponding fluorescent intensities and FRET efficiency of the RNA probe with 8 μM MBP-DDX3X (upper) and MBP-DDX3Y (lower) and 1 mM ATP, which show dynamic FRET presumably due to kinetics of dissociation and reassociation of the protein.

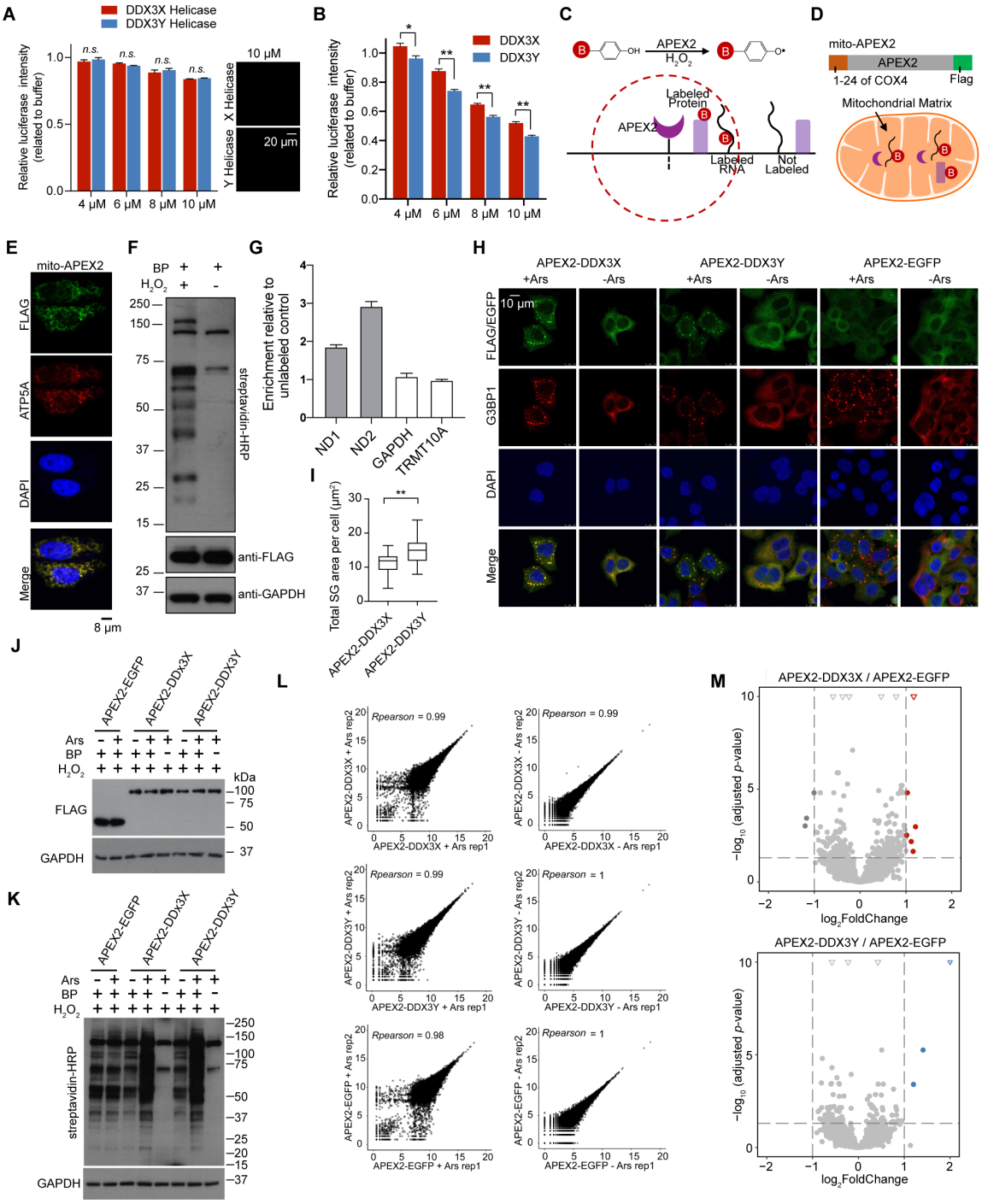
A
DDX3X Helicase
DDX3Y Helicase
Relative luciferase intensity (related to buffer)
n.s.
4 μM 6 μM 8 μM 10 μM
10 μM
X Helicase
Y Helicase
20 μm
B
DDX3X
DDX3Y
Relative luciferase intensity (related to buffer)
*
**
4 μM 6 μM 8 μM 10 μM
C
APEX2
H2O2
Labeled Protein
APEX2
Labeled RNA
Not Labeled
D
mito-APEX2
APEX2
1-24 of COX4
Flag
Mitochondrial Matrix
E
mito-APEX2
FLAG
ATP5A
DAPI
Merge
8 μm
F
BP
H2O2
250
150
75
50
37
25
15
streptavidin-HRP
anti-FLAG
anti-GAPDH
G
Enrichment relative to unlabeled control
ND1
ND2
GAPDH
TRMT10A
I
Total SG area per cell (μm²)
**
APEX2-DDX3X
APEX2-DDX3Y
H
APEX2-DDX3X
APEX2-DDX3Y
APEX2-EGFP
+Ars
-Ars
10 μm
FLAG/EGFP
G3BP1
DAPI
Merge
J
APEX2-EGFP
APEX2-DDX3X
APEX2-DDX3Y
Ars
BP
H2O2
kDa
100
75
50
37
FLAG
GAPDH
K
APEX2-EGFP
APEX2-DDX3X
APEX2-DDX3Y
Ars
BP
H2O2
250
150
100
75
50
37
25
20
15
streptavidin-HRP
GAPDH
L
Rpearson = 0.99
APEX2-DDX3X + Ars rep2
APEX2-DDX3X + Ars rep1
Rpearson = 0.99
APEX2-DDX3X - Ars rep2
APEX2-DDX3X - Ars rep1
Rpearson = 0.99
APEX2-DDX3Y + Ars rep2
APEX2-DDX3Y + Ars rep1
Rpearson = 1
APEX2-DDX3Y - Ars rep2
APEX2-DDX3Y - Ars rep1
Rpearson = 0.98
APEX2-EGFP + Ars rep2
APEX2-EGFP + Ars rep1
Rpearson = 1
APEX2-EGFP - Ars rep2
APEX2-EGFP - Ars rep1
M
APEX2-DDX3X / APEX2-EGFP
−log10 (adjusted p-value)
log2FoldChange
APEX2-DDX3Y / APEX2-EGFP
−log10 (adjusted p-value)
log2FoldChange

Figure S5 DDX3X and DDX3Y condensation inhibit the translation of luciferase RNA, and DDX3X- and DDX3Y-positive SGs have shared and unique RNA constituents in cells. Related to Figure 5. (A) Quantification of translation inhibition in the presence of the mCherry-tagged protein truncation variants (which contain only the helicase domains of DDX3X or DDX3Y) at the indicated concentrations. Error bars represent s.d. from three biological repeats at each condition. Images below the graph did not reveal noticeable phase separation in the reticulocyte assay at 10 μM DDX3; scale bar, 10 μm. (B) The *in vitro* translation assays performed at the same conditions as in Figure 5B except with the addition of 1 mM ATP. (C) Schematic illustration of APEX2-mediated proximity labeling reaction and spatial labeling of RNAs and proteins. (D) Schematic illustration of mito-APEX2 fusion system in the mitochondrial matrix. APEX2 fusion with the first 24 amino acids from mitochondrial protein COX4 allowed us to validate the APEX2-proximity labeling method used in the experiments shown in Figure 5G. (E) Representative images of co-localization of mito-APEX2 with ATP5A (a mitochondrial protein). (F) Western blots show the APEX2 labeling using an anti-biotin antibody. Proximity labeling only occurred in the presence of both BP and hydrogen peroxide. Bands at 130, 75, and 72 kDa are endogenous biotinylated proteins. BP: biotin phenol. (G) RT-qPCR quantification of cytosolic (*GADPH* and *TRMT10A*) and mitochondrial (*ND1* and *ND2*) transcripts in APEX-RNA labeling experiments. (H) Representative images of localization of APEX2-DDX3X, APEX2-DDX3Y, or APEX2-EGFP with G3BP1 in HeLa cells before and after arsenite treatment (500 μM, 1 hr). Scale bar, 10 μm. (I) Box plot of the total SG area of APEX2-DDX3X- or APEX2-DDX3Y-positive SGs per cell across 20 cells upon arsenite treatment (500 μM, 1 hr); (20 cells each from 3 biologically independent experiments). *p* values were determined by two-tailed t-test; ** $p < 0.01$. (J) Western blot results showing the expression of APEX2-EGFP, APEX2-DDX3X, and APEX2-DDX3Y in HeLa cells. (K) Western blot results showing the APEX2 labeling using an anti-biotin antibody. Ars: arsenite; BP: biotin phenol. (L) Correlation between the biological repeats of APEX-seq samples including

APEX2-DDX3X, APEX2-DDX3Y, APEX2-EGFP with (left) and without arsenite (right) treatment. (M) Top, a volcano plot showing differential RNA enrichment in streptavidin pull-downs from APEX2-DDX3X expressing cells compared to APEX2-EGFP expressing cells without 500 μM arsenite treatment. Differentially expressed genes are shown in red for APEX2-DDX3X-enriched RNAs (adjusted $p < 0.05$, $\log_2$ fold change > 1) and dark gray for APEX2-DDX3X-depleted RNAs (adjusted $p < 0.05$, $\log_2$ fold change < -1). Bottom, the corresponding volcano plot for APEX2-DDX3Y expressing cells. Differentially expressed genes are shown in blue for APEX2-DDX3Y-enriched RNAs (adjusted $p < 0.05$, $\log_2$ fold change > 1). The rest of the RNAs (which do not fit the criteria of the differential expression with $\log_2$ fold change < -1 or $\log_2$ fold change > 1, adjusted $p < 0.05$) are shown in light gray for both DDX3X and DDX3Y. The triangles represent the transcripts with $\log_2$ fold change > 2 in the X-axis; $-\log_{10}$ adjusted p >10 in the Y-axis. Of note, without arsenite treatment, APEX2-DDX3X, APEX2-DDX3Y and APEX2-EGFP are diffuse in the cytoplasm as shown in Figure S5H. Therefore, there are no significantly enriched transcripts by APEX2-DDX3X and APEX2-DDX3Y in comparison to APEX2-EGFP in the no arsenite treated condition.

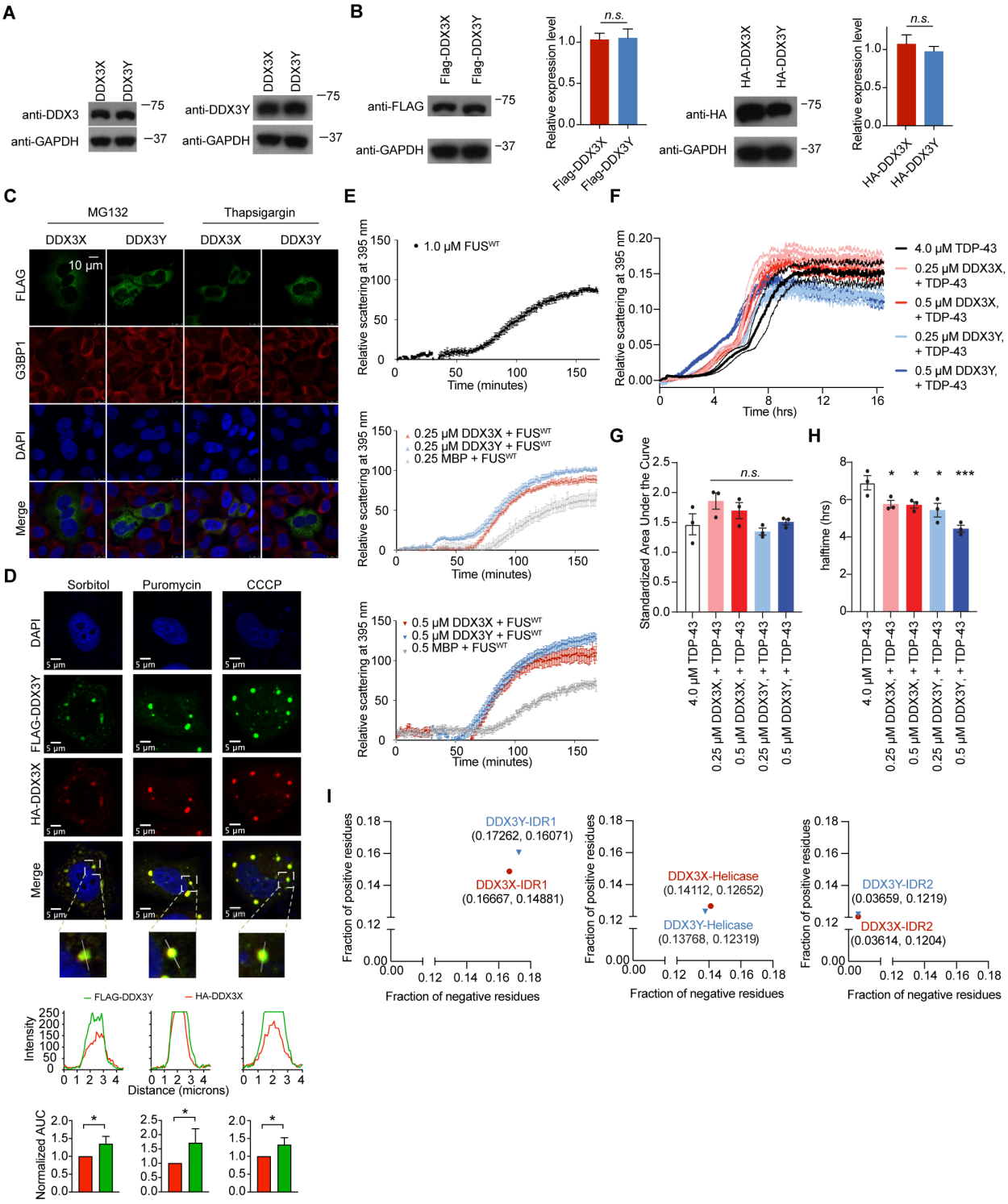
A
DDX3X
DDX3Y
anti-DDX3
anti-GAPDH
anti-DDX3Y
B
Flag-DDX3X
Flag-DDX3Y
anti-FLAG
Relative expression level
n.s.
HA-DDX3X
HA-DDX3Y
anti-HA
C
MG132
Thapsigargin
FLAG
G3BP1
DAPI
Merge
10 μm
D
Sorbitol
Puromycin
CCCP
FLAG-DDX3Y
HA-DDX3X
Intensity
Distance (microns)
Normalized AUC
E
1.0 μM FUS^WT
Relative scattering at 395 nm
Time (minutes)
0.25 μM DDX3X + FUS^WT
0.25 μM DDX3Y + FUS^WT
0.25 MBP + FUS^WT
0.5 μM DDX3X + FUS^WT
0.5 μM DDX3Y + FUS^WT
0.5 MBP + FUS^WT
F
Time (hrs)
4.0 μM TDP-43
0.25 μM DDX3X, + TDP-43
0.5 μM DDX3X, + TDP-43
0.25 μM DDX3Y, + TDP-43
0.5 μM DDX3Y, + TDP-43
G
Standardized Area Under the Curve
H
halftime (hrs)
I
DDX3Y-IDR1
(0.17262, 0.16071)
DDX3X-IDR1
(0.16667, 0.14881)
Fraction of positive residues
Fraction of negative residues
DDX3X-Helicase
(0.14112, 0.12652)
DDX3Y-Helicase
(0.13768, 0.12319)
DDX3Y-IDR2
(0.03659, 0.1219)
DDX3X-IDR2
(0.03614, 0.1204)

Figure S6 A combination of DDX3X and DDX3Y shows a stronger propensity of LLPS and translation repression than DDX3X alone, and DDX3Y enhances FUS aggregation and accelerates TDP-43 aggregation more than DDX3X. Related to Figure 6. (A) Western blot showing the expression of FLAG-DDX3X or FLAG-DDX3Y using anti-DDX3 (Abcam ab196032, left) or anti-DDX3Y (Invitrogen PA5-22050, right) antibodies. The results showed that neither of the antibodies distinguished DDX3X from DDX3Y. (B) Western blots showing the expression of FLAG-DDX3X, HA-DDX3X, FLAG-DDX3Y, HA-DDX3Y using anti-FLAG or anti-HA antibodies. The intensity of each band was quantified using Fiji. The intensity of each DDX3X or DDX3Y band was normalized to the corresponding GAPDH intensity and then normalized to the DDX3X samples. Error bars represent s.d. of three biological replicates. *P* values were determined by a two-tailed t-test; *n.s.* $p > 0.05$. (C) Immunofluorescence images of FLAG-DDX3X, FLAG-DDX3Y, and G3BP1 in Hela cells treated with MG132 (proteasome inhibitor, 10 μM, 3 hrs) or Thapsigargin (potent inhibitor of sarco/endoplasmic reticulum Ca^{2+}-ATPases, 10 μM, 1 hr). Under these conditions, we did not detect SG formation. Scale bar, 10 μm. (D) Reciprocal immunofluorescence images of SGs containing both HA-DDX3X and FLAG-DDX3Y in HeLa cells treated as the same as in Figure 6A. Below each image, traces of fluorescence intensity profiles through positions denoted by the white lines in the merged images. AUC normalized to that of HA-DDX3X is plotted for each intensity profile and shows that the signal from FLAG-DDX3Y is consistently higher than the signal from HA-DDX3X. (E) The impact of DDX3X and DDX3Y on FUS aggregation was measured using a Tecan plate reader measuring scattering at 395 nm. The indicated concentration of MBP-TEV-DDX3X, MBP-TEV-DDX3Y, or MBP (or buffer alone) was incubated with 1 μg TEV protease for 30 min at room temperature to generate untagged DDX3X and DDX3Y. 1 μM GST-TEV-FUS (or an equal volume of elution buffer, see methods) was then added to the reaction, and turbidity was used to assess aggregation by measuring scattering at 395 nm. (F) The impact of DDX3X and DDX3Y on TDP-43 aggregation was measured using a Tecan plate reader measuring scattering at 395 nm. The indicated concentrations of MBP-TEV-DDX3X or

MBP-TEV-DDX3Y, or an equal volume of elution buffer (200 mM NaCl, 25 mM Tris-HCl pH 8.0) for conditions without either protein, was incubated in TDP-43 assay buffer (150 mM NaCl, 20 mM HEPES-NaOH pH 7.0, and 1 mM DTT) with 0.5 µg TEV protease for 30 minutes at room temperature to generate untagged DDX3X and DDX3Y. Turbidity was assessed by measuring scattering at 395 nm. 4.0 µM TDP-43 (or an equal volume of TDP-43 assay buffer) was then added to the reaction, and turbidity was measured for an additional 16 hours (n = 3; dotted lines of corresponding colors represent ± s.e.m.). (G) Area under the curve of the individual replicates summarized in Figure S6F was used to compare the extent of aggregation for each condition (one-way ANOVA comparing to the 4.0 µM TDP-43 condition, Dunnett's multiple comparisons test, ± s.e.m., *n.s.* means $p > 0.05$). (H) The $t_{1/2}$ of aggregation was used to compare the kinetics of aggregation for each condition. The $t_{1/2}$ was obtained by performing nonlinear regression (asymmetric sigmoidal) on the individual replicates summarized in Figure S6F from the time of TDP-43 addition (t = 31 min) through the end of the assay (t = 16.5 hrs). Decreased halftime values indicate that both DDX3X and DDX3Y accelerate TDP-43 aggregation (one-way ANOVA comparing to the 4.0 µM TDP-43 condition, Dunnett's multiple comparisons test, ± s.e.m., $*p < 0.05$ and $***p < 0.001$). (I) The fraction of negative and positively charged amino acids in the IDR1, IDR2, and helicase domain of DDX3X (red) or DDX3Y (blue). The fractions were calculated using numbers of the charged residues over the total number of amino acids in the individual domains via CIDER software.

Table S1. Summary of smFRET values, related to Figure 4.

	Relative area of Low FRET peak	Average low-FRET Efficiency	Average high-FRET Efficiency
RNA probe only	1	0.124 (0.120, 0.127)	NA
8 μM MBP	0.933 (0.877, 0.970)	0.164 (0.156, 0.172)	0.789 (0.656, 0.816)
8 μM MBP + DDX3X/3Y	0	NA	0.807 (0.800, 0.814)
2 μM DDX3X	NA	NA	0.841 (0.830, 0.850)
4 μM DDX3X	NA	NA	0.822 (0.819, 0.825)
8 μM DDX3X	NA	NA	0.818 (0.814, 0.822)
2 μM DDX3Y	NA	NA	0.845 (0.834, 0.851)
4 μM DDX3Y	NA	NA	0.811 (0.808, 0.814)
8 μM DDX3Y	NA	NA	0.819 (0.815, 0.824)
2 μM DDX3X + ATP	0.061 (0.022, 0.10)	0.010 (-0.0097, 0.032)	0.836 (0.827, 0.844)
4 μM DDX3X + ATP	0.249 (0.218, 0.285)	-0.0039 (-0.0081, - 0.00074)	0.840 (0.834, 0.845)
8 μM DDX3X + ATP	0.41 (0.37, 0.45)	-0.010 (-0.014, - 0.0062)	0.819 (0.812, 0.825)
2 μM DDX3Y + ATP	0.019 (0.013, 0.034)	0.001612 (0.001608, 0.001671)	0.85 (0.84, 0. 86)
4 μM DDX3Y + ATP	0.161 (0.130, 0.185)	-0.0064 (-0.011, - 0.0019)	0.818 (0.813, 0.822)
8 μM DDX3Y + ATP	0.23 (0.20, 0.26)	-0.0077 (-0.012, - 0.0031)	0.824 (0.816, 0.830)

"NA" indicates the absence of the corresponding peak.
The values in the parentheses are the 95% confidence intervals of the indicated value.